Journal of Catalysis 278 (2011) 111–122

Contents lists available at ScienceDirect

Journal of Catalysis

journal homepage: www.elsevier.com/locate/jcat

High-surface thermally stable mesoporous gallium phosphates constituted by nanoparticles as primary building blocks

Vasile I. Parvulescu [a,*], Viorica Parvulescu [b], Dragos Ciuparu [c], Christopher Hardacre [d], Hermenegildo Garcia [e,*]

[a] Dept. Chemical Technology and Catalysis, University of Bucharest, B-dul Regina Elisabeta 4-12, Bucharest 030016, Romania
[b] Institute of Physical Chemistry of the Romanian Academy, 202 Splaiul Independentei St., P.O. Box 194, 060021 Bucharest, Romania
[c] Petroleum-Gas University of Ploiesti, Bd. Bucureşti 39, Ploieşti, Romania
[d] School of Chemistry and Chemical Engineering, Queen's University, Stranmillis Road, BT9 5AG Belfast, UK
[e] Instituto de Tecnologia Quimica CSIC-UPV, Universidad Politecnica de Valencia, Av. De los Naranjos s/n, Valencia 46022, Spain

ARTICLE INFO

Article history:
Received 22 June 2010
Revised 9 November 2010
Accepted 29 November 2010
Available online 15 January 2011

Keywords:
High surface gallophosphate
Thermally stable gallophosphate
Sol–gel route
Toluene oxidation

ABSTRACT

In constant, search for micro/mesoporous materials, gallium phosphates, have attracted continued interest due to the large pore size reported for some of these solids in comparison with analogous aluminum phosphates. However up to now, the porosity of gallium phosphates collapsed upon template removal or exposure to the ambient moisture. In the present work, we describe high-surface thermally stable mesoporous gallium phosphates synthesized from gallium propoxide and PCl_3 and different templating agents such as amines (dipropylamine, piperidine and aminopiperidine) and quaternary ammonium salts ($C_{16}H_{33}(CH_3)3NBr$ and $C_{16}PyCl$). These highly reactive precursors have so far not been used as gallium and phosphate sources for the synthesis of gallophosphates. Conceptually, our present synthetic procedure is based on the fast formation of gallium phosphate nanoparticles via the reaction of gallium propoxide with PCl_3 and subsequent construction of the porous material with nanoparticles as building blocks. The organization of the gallophosphate nanoparticles in stable porous structures is effected by the templates. Different experimental procedures varying the molar composition of the sol–gel, pH and the pretreatment of gallium precursor were assayed, most of them leading to satisfactory materials in terms of thermal stability and porosity. In this way, a series of gallium phosphates with surface are above 200 $m^2 g^{-1}$, and narrow pore size from 3 to 6 nm and remarkable thermal stability (up to 550 °C) have been prepared. In some cases, the structure tends to show some periodicity and regularity as determined by XRD. The remarkable stability has allowed us to test the catalytic activity of gallophosphates for the aerobic oxidation of alkylaromatics with notable good results. Our report reopens the interest for gallophosphates in heterogeneous catalysis.

1. Introduction

The synthesis of porous phosphates received much interest since Wilson et al. discovered the microporous crystalline aluminophosphates [1]. Soon after that, Parise [2–5] extended the synthesis of these phosphates to gallium phosphates. Structural analogues of AlPO molecular sieves were synthesized using the structure-directing agent protocol [6]. Over the time, a large family of open-framework phosphate-based structures has been reported [7] of which gallium phosphates were extensively investigated. Since the first structures were synthesized [2], the exploration of gallophosphates via the fluoride method [8] led to the discovery of a large architectural diversity of open-framework structures including the extra-large pore cloverite [9] and DIPYR-GaPO [10] structures, the Mu-n [11–14], ULM-n [15] or cyclam-GaPO [16] types. In these solids, gallium can adopt 4-, 5- or 6-fold coordination.

Different routes have been used to prepare gallium phosphates [17] such as the hydrothermal treatment of a gallophosphate mixture containing water, an organic structure-directing agent and fluoride. Fluoride was found in the synthesized material as terminal Ga–F groups or occluded in small structural units, acting as a stabilizer of the building units [18]. Among the preparative variables considered to improve the stability of these materials were the nature of gallium and phosphorous precursors. In most of the studies, Ga_2O_3 or GaO(OH) was considered as a gallium source and H_3PO_4 or P_2O_5 as a phosphorous source [19]. Ionothermal synthesis of microporous gallium phosphates [20,21] has also been reported for LTA structures. These syntheses were carried out via a

* Corresponding authors. Tel./fax: +40 745502052 (V.I. Parvulescu), +34 963877809 (H. Garcia).
E-mail addresses: vasile.parvulescu@g.unibuc.ro (V.I. Parvulescu), c.hardacre@qub.ac.uk (C. Hardacre), hgarcia@qim.upv.es (H. Garcia).

0021-9517/$ - see front matter © 2010 Elsevier Inc. All rights reserved.
doi:10.1016/j.jcat.2010.11.021

hydrothermal treatment using an ionic liquid (IL) [[Emim]Br or a deep-eutectic solvent composed of choline chloride and tetrahydro-2-pyrimidinone] as structure-directing agent and fluorhydric acid. These results indicated that higher reaction temperature was beneficial to crystal formation and attributed this effect to the lower viscosity of IL and high growth ratio of the crystal at the optimized temperature.

Experiments done by Caro's group [22] for the synthesis of $GaPO_4$-LTA following Kessler's method [23] showed that under the applied hydrothermal conditions, the first stage is the formation of quartz-type $GaPO_4$ that then transforms into zeotype $GaPO_4$-LTA.

Nevertheless, several works also described the preparation of gallium phosphates in the absence of fluorine [24]. Wragg and Morris [25] reported the synthesis of a gallium phosphate D4R unit containing occluded oxygen by a solvothermal method using a mixture of pyridine and water as the solvent. It shows an ionic structure containing discrete $[H_8Ga_4P_4O_{21}]^{2-}$ anions hydrogen-bonded into an open structure with pyridinium ions as the charge balancing cations. This structure was obtained using phosphoric acid, gallium sulfate, and pyridine as reactants. Surprisingly, similar synthetic procedures containing fluoride failed to form materials containing the D4R unit.

Various mesoporous oxides, sulfides, and phosphates have been synthesized based on surfactant templating strategy [26–28]. It is usually considered that synthesis of these materials follows different self-assemble mechanisms, and templates used in the preparations could control their structures and morphologies [29–31]. Therefore, choice of templates becomes a key issue for synthesis of these mesoporous materials. The organic templates used to prepare ordered gallium phosphates structures led to a wide range of atomic arrangement types including isolated clusters, chainlike structures, layered networks and three dimensional frameworks [24]. Among the various organic structure-directing agents, diaminoalkanes exhibit the strongest templating effect [32]. Amphiphilic triblock copolymer F127, $[(EO)_{106}(PO)_{70}(EO)_{106}]$–OH was also reported in the synthesis of gallium phosphate using a hydrothermal route [25].

In contrast with zeolitic aluminosilicates or aluminophosphates, the removal of template from gallium phosphates is in most cases accompanied by a collapse of the inorganic framework. This has hampered up to now any possibility to use porous gallophosphates in heterogeneous catalysis. Computer simulation to analyze various gallophosphate forms of zeolites confirmed the instability of these structures upon template loss, unlike their aluminophosphate counterparts [33]. Therefore, only very few GaPO structures were reported to exhibit any thermal stability [7]. Recent studies confirmed important changes of the lattice parameter of gallium phosphate with respect to temperature [34,35].

The instability of the gallium phosphates toward moist air suggested an inherently different flexibility of the network that allows easy coordination of water and a low-temperature phase transition to lower symmetry in these structures [35]. However, most of these host frameworks involve OH groups or H_2O molecules so that they are not really pure oxides [36].

Another attempt to prepare gallium phosphates is that proposed by Bonhomme et al. [37] which refers to the synthesis of a 3D-gallophosphate $(NH_4)_3Ga_2(PO_4)_3$. These structures can be prepared using hydrothermal synthesis from Ga_2O_3 and $(NH_4)_2HPO_4$ and consist of GaO_5 bipyramid and PO_4 tetrahedron units. They are indeed microporous materials, but also with a weak thermal stability.

Zeolites and other micro- and mesoporous materials have important applications as adsorbents, solid catalysts as well as rigid host frameworks which include guest species [38,39]. Besides the field of heterogeneous catalysis and inclusion materials, there are also some emerging potential applications of porous materials in nanotechnology to develop solar cells, electroluminescent devices and sensors [40–44]. In all these fields, there is a continuous need for novel high surface area, stable porous hosts that can overcome the limitations of the current materials in terms of limited available pore sizes, difficult synthesis, controlled crystal morphology and ability to form thin films. Considering the diversity of structures of pore size range, gallium phosphates can complement and fill a gap currently not covered by porous aluminosilicates. However, up to now and as it has been commented above, the structural instability of gallophosphates has impeded any application of these materials in heterogeneous catalysis or nanotechnology, remaining them as a simple curiosity.

In view of what precedes, the aim of the present work was to investigate the synthesis of thermally stable mesoporous gallium phosphates and their application as heterogeneous catalysts. Our approach has been to use totally unexplored new gallium and phosphate sources that are considerably more reactive than those used before, expecting that this high reactivity will transform these molecular compounds into small nanoparticles that will act as the real building blocks of the porous material. The effects of various organic templates like quaternary ammonium salts and amines on the synthesis and properties of gallium phosphate were studied. The template effect of amines for materials with metals of the same periodic table group was reported in the synthesis of phosphates like indium [45] or aluminum phosphates [46] These precedents encouraged us to use different amines as templates for the synthesis of gallium phosphates. The data presented below firmly support that our concept is of general use and can serve to finally develop porous gallophosphate with activity as heterogeneous catalysts.

2. Experimental methods

Mesoporous gallium phosphates were synthesized by two sol–gel protocols. The differences between these procedures result from the pretreatment of the gallium precursor, the nature of the template and the molar composition of the sol–gel. In both syntheses, gallium iso-propoxide (AlfaAesar) and PCl_3 (AlfaAesar) were used as precursors. In the first protocol, 70 mL solution of 0.224 M $Ga(OC_3H_7)_3$ in mixture of THF and propanol (molar ratio 1:2) was refluxed at 70 °C for 3 h, cooled at room temperature, and mixed with 1.95 g of PCl_3 under vigorous stirring. To the resulting solution, one of the following templates or their solutions was added drop-wise: (i) dipropylamine till a pH of 6–7 was reached (GM1); (ii) an alcoholic solution of $C_{16}H_{33}(CH_3)_3NBr$ obtained by dissolving 3.2 g of $C_{16}H_{33}(CH_3)_3NBr$ in 20 g of *n*-propanol (GM2); (iii) an alcoholic solution of N-cetylpyridinium chloride ($C_{16}PyCl$) obtained by dissolving 1.52 g of $C_{16}PyCl$ in 20 g of 2-propanol (GM3); and (iv) finally, an aqueous suspension of $C_{16}PyCl$ obtained by mixing of 1.52 g $C_{16}PyCl$ in 20 g H_2O. The pH was adjusted at 6–7 by adding 25% aqueous solution of $(CH_3)_4NOH$ (GM4).

In contrast to the previous protocol using quasi-neutral conditions, in the second protocol, acetic acid was used to decrease the pH of the gel solution. Thus, 75 mL of *n*-butyl alcohol was added to 70 mL of a 0.12 M solution of $Ga(OC_3H_7)_3$ in THF. To this solution, 2.53 g of PCl_3 was added under vigorous stirring. After 1 h, the resulting solution was treated with 6 mL of CH_3COOH and stirred vigorously for 23 h. Then, 2.95 g of piperidine (GM-5) or 2.85 g of 4-aminopiperidine (GM6) was added and mixed for 3 h. Table 1 compiles the preparation conditions in which these materials have been synthesized.

All mixtures were autoclaved in a microwave-oven for 1 h at 60 °C, then 1 h at 80 °C and finally 3 h at 100 °C. The obtained

Table 1
Synthesis conditions of six gallophosphates prepared in this work.

Sample	Surfactant	Ga:P:s:t:a:w[a] Molar ratio of the gel	pH	Solvents of precursors/surfactant
GM1	Dipropylamine	1.0:1.0:2.4:1.9:20.0:0	6–7	THF-*n*-propanol no solvent
GM2	$C_{16}H_{33}(CH_3)_3NBr$	1.0:1.0:0.6:1.9:38.7:0	6–7	THF-*n*-propanol/*n*-propanol
GM3	$C_{16}PyCl$	1.0:1.0:0.3:1.9:38.7:0	6–7	THF-*n*-propanol/2-propanol
GM4	$C_{16}PyCl$	1.0:1.0:0.3:1.9:20.0:78.2	6–7	THF-*n*-propanol/water
GM5	Piperidine	1.0:2.2:4.1:47.9:108.6:0	3	THF-*n*-butanol-acetic acid/no solvent
GM6	Amino-piperidine	1.0:2.2:3.3:47.9:108.6:0	3	THF-*n*-butanol-acetic acid/no solvent

[a] Ga: Ga(OC3H7); P: PCl3; s: surfactant, t: THF, a: alcohol (*n*-propanol or *n*-butanol), w: water.

solids were washed in distilled water, dried at 110 °C under vacuum, and then gently calcined 6 h at 550 °C (rate 0.6 °C per minute). This temperature corresponds to the thermal stability of these materials.

The resulting materials were characterized using elemental analysis, nitrogen adsorption–esorption isotherms at −196 °C, thermal analysis, XRD, XPS, CP/MAS ^{71}Ga and ^{31}P NMR, in situ FTIR, SEM, TEM and EXAFS.

The elemental analysis was conducted on a Perkin–Elmer 2400 elemental analyzer. Inductively coupled plasma analysis was performed on a Perkin–Elmer Optima 3300DV ICP instrument. Nitrogen contents were determined by combustion analysis using a LECO equipment. Thermal analysis was performed with a TGA (Perkin–Elmer Pyris Diamond TG/DTA apparatus) using ∼10 mg samples heated in platinum or alumina crucibles at 10 °C min^{-1}.

Gas adsorption measurements were performed with a Micromeritics ASAP 2020 sorption analyzer. Surface areas have been obtained by N_2 adsorption at the nominal temperature of liquid nitrogen (−196 °C) on all materials previously out-gassed at 120 °C in vacuum for 12 h. The specific surface areas and the pore size distributions were calculated from the Brunauer–Emmett–Teller (BET) equation and from the adsorption isotherm using the Barrett–Joyner–Halenda (BJH) method, respectively.

Powder X-ray diffraction (XRD) patterns were recorded on a Siemens D 5000 diffractometer using the Cu Kα radiation (wavelength 1.5406 Å). The patterns were collected ranging 2θ from 1.5° to 75° with a step size of 0.1° and a time step of 1.0 s. XPS spectra were recorded at room temperature using a SSX-100 spectrometer, Model 206 from Surface Science Instrument. The pressure in the analysis chamber during the analysis was 1.33 mPa. Monochromatized Al Kα radiation ($h\nu$ = 1486.6 eV) was used. It was generated by bombarding the Al anode with an electron gun operated with a beam current of 12 mA and acceleration voltage of 10 kV. The spectrometer energy scale was calibrated using the Au $4f_{7/2}$ peak centered at 83.98 eV. Charge correction was made with the C 1s signal of adventitious carbon (C–C or C–H bonds) located at 284.8 eV. An estimated error of ±0.1 eV can be assumed for all measurements.

FTIR spectra were collected with a Nicolet 4700 IR spectrometer from ThermoElectron. The samples were compressed into self-supporting disks (10–15 mg cm^{-2}). Spectra were collected at room temperature at a resolution of 1 cm^{-1} using 50 scans for each measurement. A background spectrum was recorded before measurements. This was automatically subtracted, and the reported spectra are the result of the subtraction.

CP/MAS ^{71}Ga and ^{31}P NMR spectra were collected with a Bruker Avance 750 MHz spectrometer, at room temperature, using a 4-mm double resonance probe head. The sample holder was spun with a frequency up to 15 kHz. Chemical shifts for ^{71}Ga resonances were referred to the ^{71}Ga resonance of external $Ga(NO_3)_3$ 1 M, while for ^{31}P resonances chemical shifts were referred to the ^{31}P resonance of H_3PO_4 85% solution. The spectra deconvolution was made employing Dmfit [1] program.

X-ray absorption data were collected at beam line X18B, National Synchrotron Light Source, Brookhaven National Laboratory. The beamline is equipped with a Si(1 1 1) channel cut monochromator with detuning and deglitching capabilities. Two ion chambers were placed coaxially with the beam, in front and behind the sample, to measure the intensities of the incident (I_0) and transmitted (I_T) beams. A third ion chamber was used to record the spectrum of the internal reference sample consisting of a gallium foil in order to determine the absorption edge of Ga (10,367 eV) for each spectrum. Approximately 45 mg sample was pressed into a rectangular wafer (ca. 1.5 × 1 cm) to form 0.5-mm-thick pellets. The thickness of pellets satisfied the condition that the absorption edge step, $\Delta\mu x$, at the Ga K absorption edge was smaller or equal to 1. Extended X-ray Absorption Fine Structure (EXAFS) spectra were recorded in the transmission mode from 200 eV below to 1000 eV above the Ga K edge. The analysis of the X-ray adsorption spectra followed the procedures described in detail in previous contributions [47]. The EXAFS spectra were calibrated to the edge energy of the gallium foil internal reference. The background removal and edge-step normalization were performed using the FEFFIT code [48].

High-Resolution Transmission Electron Microscopy (HR-TEM) images of the samples were collected on a Tecnai F20 200 kV microscope from Philips. The instrument is equipped with a field emission gun and provides accelerating voltages of up to 200 kV. The point resolution and the line resolution were 0.24 and 0.12 nm, respectively, at a focal length of 1.7 mm. The solid samples were dispersed in pure ethanol by sonication, and approximately 0.05 ml of this suspension was dropped on a copper mesh coated with an amorphous holey carbon film. The ethanol evaporated at room temperature prior to the TEM analysis performed at 200 kV accelerating voltage. The Fourier transform was obtained using the tools of the Gatan software package for TEM data acquisition and processing. Scanning electron microscopy (SEM) was performed using a Philips XL-20 microscope.

Aerobic oxidation of toluene using GM gallophosphates as solid catalysts were carried out in a magnetically stirred 50-mL Teflon-lined autoclave, equipped with an electric furnace and a temperature control with a sensibility of 0.2 °C. Typical reaction conditions used 0.12 mol toluene and 0.3 g catalyst. After the temperature reached 150 °C, under a continuous stirring, oxygen was charged to the reactor at a pressure of 3 bar. The pressure was kept constant during the reaction (4 h) by supplying additional volume of oxygen gas. Prior to reaction, the catalyst was calcined under helium flow (30 mL cm^{-3}) at 300 °C for 2 h. The reaction products were analyzed by a GC–MS Thermo Electron Trace GC–DSQ system after the separation of the catalysts by filtration. The conversion and product distribution were evaluated with calibration curves.

3. Results

As commented in the introduction, our synthesis of $GaPO_4$ relies in the use as precursors of gallium propoxide and phosphorous

trichloride. These precursors have not been previously used in the preparation of gallophosphates. After contacting these two precursors, a structure-directing agent is added under quasi-neutral pH (GM1–4) or under acidic conditions (GM5 and GM6). Table 1 indicates the codes of the six samples under study and summarizes the synthesis conditions employed in the preparation of each material. The template method is usually considered as a general methodology to design and synthesize ordered mesoporous solids. With aim of modifying the porosity and structure of $GaPO_4$, we selected one common amine (dipropylamine) and two less common amines as piperidine and 4-aminopiperidine (firstly reported as template for the synthesis of oxides in this paper). As it will be demonstrated below, the properties of the resulting phosphates were influenced by the nature of the quaternary ammonium salts, the type of the cations ($C_{16}H_{33}(CH_3)_3NBr$ and $C_{16}PyCl$), the solvent (alcohol or water) and organic electrolyte ($(CH_3)_4NOH$).

After the synthesis, we proceeded to characterize the textural and spectroscopic properties of the mesoporous gallophosphates GM1–6 with the aim to obtain information about the influence of the structure-directing agent and synthesis conditions on the properties of the resulting materials.

Table 2
Textural characteristics of the gallium phosphates after calcination at 550 °C.

Sample	Surface area ($m^2\ g^{-1}$)	Pore size (nm)	*t*-Plot micropore area ($m^2\ g^{-1}$)	Pore volume ($cm^3\ g^{-1}$)
GM1	160.0	5.8	20.0	0.40
GM2	215.0	3.9	0.0	0.32
GM3	198.0	3.7	0.0	0.22
GM4	164.0	4.0	28.0	0.31
GM5	40.0	2.3 and 10.5	3.7	0.15
GM6	180.0	3.2	0.0	0.31

3.1. Thermal analysis

Thermal analysis curves indicated for all these materials a continuous mass loss till about 385 °C. This loss corresponds to the total decomposition of the directing agent occluded within the material. The subsequent increase of the temperature till 550 °C was not accomplished by any change in the mass loss. Thus, the thermal analysis indicates that the gallophophates GM1–4 and GM5–6 are thermally stable up to temperatures above 550 °C. This high decomposition temperature is quite remarkable and unprecedented, particularly considering that the porosity of the material is maintained. The color all of the calcined materials is yellow.

3.2. Textural characterization

After template removal by calcination at 550 °C, all the GM samples exhibit porosity with notable pore volumes corresponding to mesopores with absent or minor microporosity. The isotherms of the samples measured at −196 °C were irreversible type IV isotherms according to the IUPAC with a hysteresis loop at a lower closing point at $p/p_0 = 0.42$, indicating the formation of mesopores. Table 2 compiles the textural characteristics of samples calcined at 550 °C. As it can be seen there, only samples GM1 and GM4 exhibit some significant microporosity. The nitrogen adsorption–desorption isotherms given in Fig. 1 demonstrate that the hysteresis loops depend on the nature of the surfactant and the preparation procedure. For the samples GM2 and GM3, the hysteresis loops were of the IUPAC H2-type, which is associated with a more complex pore structure in which network effects like interconnections are important (Fig. 1b and c) [49,50]. By using small surfactants, as dipropylamine for GM1, or an aqueous solution of surfactant for GM4, the shape of the loops was changed, indicating changes in the pore structure (Fig. 1a and d). This change was more evident for GM4, where the hysteresis loop better approximated the IUPAC H4-type. Hysteresis loops of type H4 are given by slid-shaped

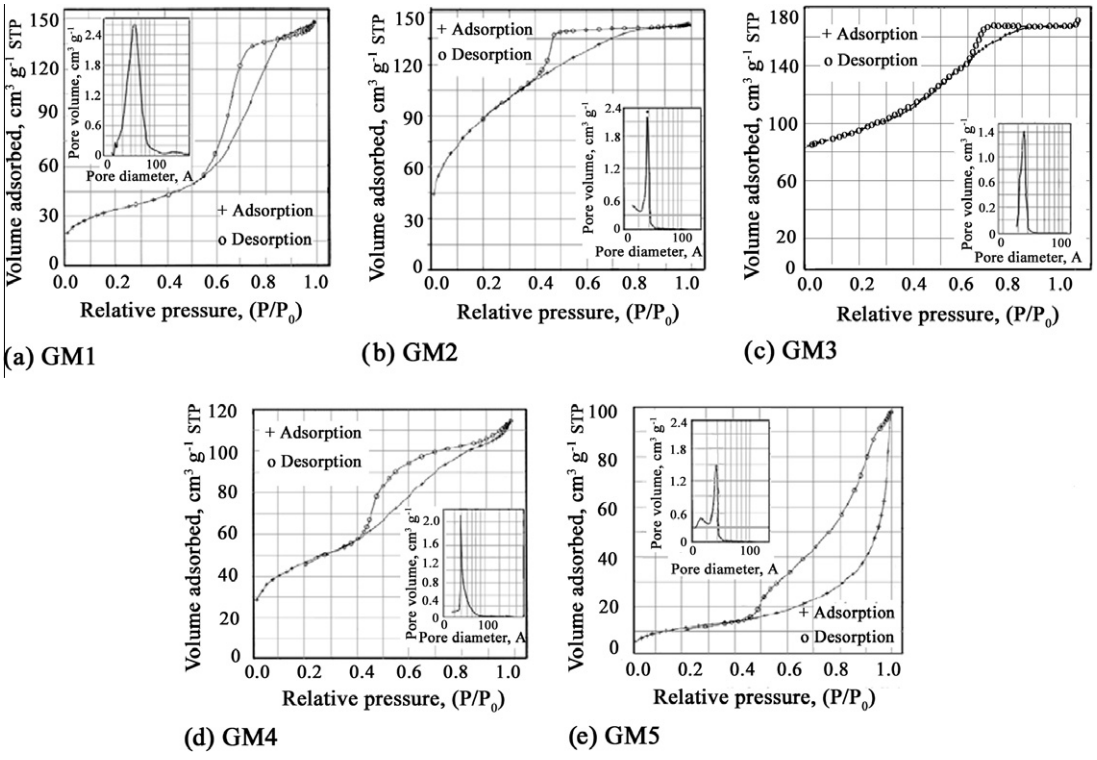

Fig. 1. Adsorption (+)/desorption (o) isotherms of the investigated samples and the pore size distribution.

pores, but in this case, the contribution of the micropores becomes important (Table 2) [51].

Concerning GM5 and GM6 prepared using acetic acid, changing both the surfactant to piperidine ones and the synthesis pH value led to a more complicate texture (Fig. 1e). Thus, the hysteresis loops for GM5 and GM6 prepared in the presence of piperidine and amino piperidine, respectively, corresponded to H3 loops usually given by aggregates of platy particles containing slit-shaped pores [51].

Regardless the actual profile of the isothermal gas adsorption what must be remarked is that all the GM samples prepared here from $Ga(OPr)_3$ and PCl_3 exhibit a remarkable narrow pore size distribution (Fig. 1).

3.3. FTIR spectra

IR spectroscopy is a useful technique to determine the functional groups present in a solid. In the present case, this spectroscopy clearly establishes the formation of phosphate anions by hydrolysis of the PCl_3 precursor. Thus, FTIR spectra (spectra not shown) presented for all the samples bands at 1076 cm^{-1} due to the vibration of P–O bonds and at 631 and 511 cm^{-1} assigned to Ga–O and O–P–O bonds, respectively, in gallium phosphate [52].

3.4. MAS NMR results

3.4.1. ^{31}P and ^{71}Ga MAS NMR spectra of GM samples

Non-calcined samples showed a ^{31}P MAS NMR resonance signal in the range −0.5 to −1.0 ppm and a shoulder at −12.0 ppm (Fig. 2, Table 3). According to Haouas et al. [53], the line at −0.5 to −1.0 ppm can be assigned to free unbound phosphoric acid, while the shoulder to tetrapodally coordinated phosphate groups. After calcining at 550 °C, the two lines shifted to around −6.0 ppm, which might indicate a reorganization of the phosphorous species around gallium, leading to the formation of bipodally coordinated gallophosphates species (Scheme 1).

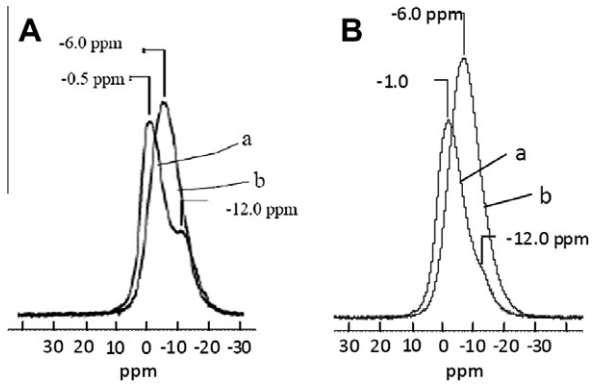

Fig. 2. ^{31}P MAS NMR spectra of GM3 (A) and GM4 (B) samples: (a) uncalcined; (b) calcined at 550 °C, recorded with a rotation frequency of 15 kHz; 950 scans.

These values rule out the formation of detectable nitride groups in the gallophosphates. According to previous studies, when nitrogen is incorporated in phosphates, the resonance signal at −14.0 ppm is shifted upfield (around −23 ppm) and its intensity decreases. Simultaneously, two other peaks appeared, centered around −5.0 and 13.0 ppm [54,55]. In the present case, only a well-centered line at −6.0 ppm was measured. Additionally, the band at 13.0 ppm typical for $P(O_2N_2)$ tetrahedra was always absent, pointing to the absence of a mild nitridation of PO_4 tetrahedra [56].

Fig. 3 gives the ^{71}Ga MAS NMR spectra of GM3 and GM4 samples. Uncalcined samples exhibit lines centered at −171, 27, 157 and 312 ppm for GM3 and −179, 20, 158 and 308 ppm for GM4, respectively (Table 3). The signal in the range 6–20 ppm is due to Ga coordinated by oxygen [53],and in this case, it can be assigned to bipodal phosphate species. Thus, the band located around 157 ppm and 20–27 ppm can surely correspond to two different coordination states of Ga in the dicoordinate phosphate, possibly $Ga(O_4)$ tetrahedra and $Ga(O_6)$ octahedra, respectively. For comparison, in oxide compounds, $Ga(O_4)$ groups give rise to a signal around 200 ppm, and $Ga(O_6)$ groups appear in the spectra around 0 ppm [45]. These two peaks in the range 160–157 and 27–20 ppms correspond to the vast majority of the Ga present in the samples, while the smaller peak at −171 ppm characteristic of 6-fold coordinated Ga corresponds to a minor population of this metal ion. By comparing with the values of −110 to 118 ppm recorded for tetracoordinated Ga site in $GaPO_4$ cristobalite [57–59], it can be proposed that the peak recorded at −174 to −179 ppm would correspond to similar tetracoordinated Ga ion in $GaPO_4$ [84].

Calcination caused just a small shift of the line centered in the range 20–27 ppm. The upfield shift from 12 to 6 ppm upon calcination of GM samples is consistent with the reorganization described in Scheme 1.

As for ^{31}P MAS NMR results, the recorded ^{71}Ga MAS NMR spectra provided no information about the insertion of nitrogen into the gallophosphate structure. This is fully consistent with the lack of significant N content in the materials as determined by chemical analysis [54].

Figs. 4 and 5, and Table 3 show the ^{31}P and ^{71}Ga MAS NMR spectra and the corresponding δ values for the GM5 and GM6 samples. In the ^{31}P MAS NMR spectra, the dried samples show a line located at −1.0 ppm, like for the GM samples, one at −27 ppm and another at 25 ppm. The band at 25 ppm is assigned to the phosphonium in a high electron coordination surrounding [60].

Table 3
Summary of the chemical shift and integral of the peaks in ^{31}P and ^{71}Ga MAS NMR spectra for GM samples.[a]

Sample	^{31}P	^{31}P	^{31}P	^{71}Ga	^{71}Ga	^{71}Ga	^{71}Ga
GM1[d]	−0.5 [69]		−12 [26]	311 [8]	157 [26]	24 [46]	−174 [12]
GM1[c]		−6.0 [100]		311 [10]	160 [29]	10 [49]	−174 [12]
GM2[d]	−0.5 [73]		−12 [27]	309 [10]	157 [30]	21 [48]	−176 [12]
GM2[c]		−6.0 [100]		309 [11]	160 [31]	7 [49]	−176 [9]
GM3[d]	−0.5 [69]		−12 [31]	312 [8]	157 [32]	27 [49]	−171 [11]
GM3[c]		−6.0 [100]		312 [9]	160 [30]	12 [49]	−171 [12]
GM4[d]	−1.0 [82]		−12 [18]	308 [11]	158 [25]	20 [51]	−179 [13]
GM4[c]		−6.0 [100]		308 [12]	160 [27]	6 [47]	−179 [14]
GM5[d]	25 [17]	−1.0 [68]		−27 [15]	308 [11]	158 [32]	20 [45]
GM5[c]			−6 [100]		308 [12]	160 [30]	6 [47]
GM6[d]	25 [19]	−1.0 [66]		−27 [15]	308 [10]	158 [33]	20 [45]
GM6[5]			−6 [100]		308 [12]	160 [31]	6 [46]

[a] The superscripts d and c correspond to dried and calcined, respectively. The number in brackets indicates the relative area of the peaks.

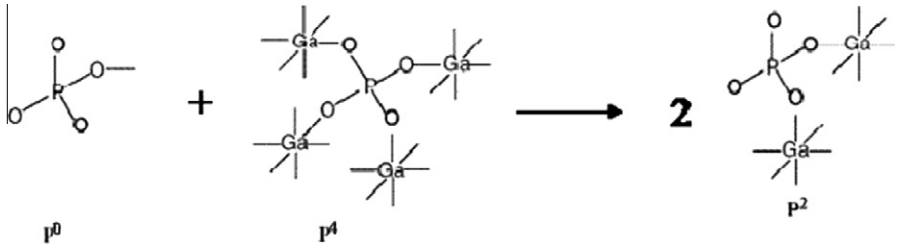

Scheme 1. Reorganization of phosphorous species during calcination with the formation of dicoordinated phosphate.

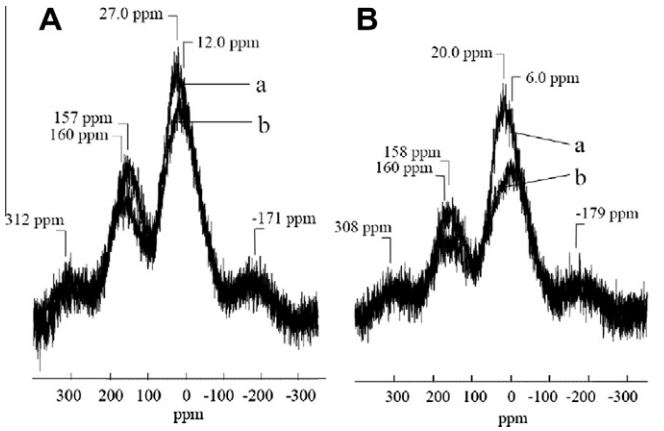

Fig. 3. ^{71}Ga MAS NMR spectra of dried (a) and calcined at 550 °C (b) GM3 (A) and GM4 (B) samples, recorded with a rotation frequency of 15 kHz and accumulating 950 scans.

The decreased value of the band at −27 ppm, by comparing with that at −12 ppm for GM1–4 samples, may account for a decreased value of the Ga–O–P bond angle in dried samples [61]. After calcination, the ^{31}P MAS NMR spectra of these samples were identical with those found for GM1–4 samples, suggesting the same reorganization of the coordination sphere around Ga as that described in Scheme 1. This reorganization is manifested by the appearance of a single band located at −6.0 ppm.

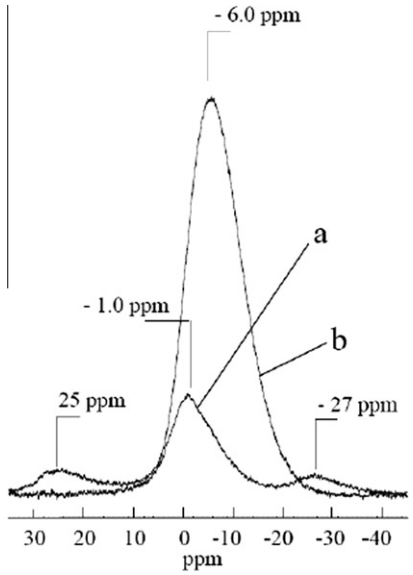

Fig. 4. ^{31}P MAS NMR spectra of dried (a) and calcined (b) at 550 °C GM6 recorded with a rotation frequency of 15 kHz using 950 scans.

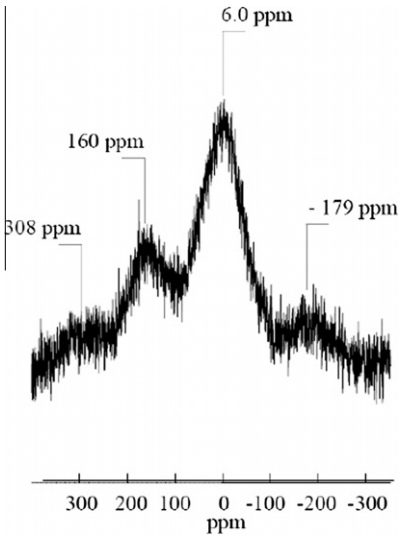

Fig. 5. ^{71}Ga MAS NMR spectra of calcined at 550 °C GM6, recorded with a rotation frequency of 15 kHz using 950 scans.

^{71}Ga MAS NMR spectra (Fig. 5) of the GM6 sample showed the same bands as for GM1–4 ones, and the calcination exhibited the same effects (Table 3).

3.5. XRD

Typical XRD patterns of GM1–4 samples are shown in Fig. 6. They correspond to materials lacking a well-defined periodic structure [52]. However, the patterns presented in Fig. 6 showed at small angles ($2\Theta < 3$) a peak characteristic for materials with some degree of ordered mesoporous structure. This peak is particularly well developed for GM4 (see Fig. 6c). It is worth commenting that the low-angle does not decrease in intensity, but shifts toward higher angles, upon calcination at 550 °C, this indicating that the structure is preserved and shrinks after the thermal treatment and equilibration to the ambient. This behavior is remarkable compared to other gallophosphates that promptly become amorphous upon template removal, especially when exposed to moisture. Structure shrinkage upon calcination is a general phenomenon in porous materials and derives from the sintering of the building blocks, typically related to structural stability. In the case of GM5 and GM6 samples, no clear low-angle diffraction peak was observed indicating their amorphous (but mesoporous) structure (see Supplementary Material).

From the XRD patterns of GM1, GM2 and GM4 and their narrow pore size distribution, it can be proposed that these gallophosphates exhibit a wormhole framework structure analogous to some mesoporous materials constituted by nanoparticles [62–64].

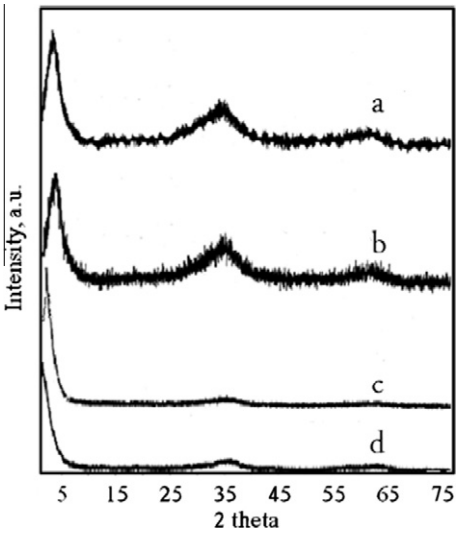

Fig. 6. XRD patterns of GM1 calcined (a), GM2 calcined (b), GM4 calcined (c), and GM4 dried (d).

3.6. EXAFS

The near-edge region of the normalized, background subtracted, and phase corrected Extended X-ray Absorption Fine Structure (EXAFS) spectrum of the synthesized GM3 sample is shown in Fig. 7a, along with the spectra recorded for commercial GaN and Ga_2O_3 samples used as reference materials. Similar spectra were obtained for all GM samples. The EXAFS spectrum of the phosphate sample in the *R* space is compared with that of the gallium oxide in Fig. 7b.

The spectrum of GM3 presents a white line, centered at 10,370.5 eV and two structures around 10,375 and 10,387.5 eV, respectively, which is in a good concordance with data reported previously by Tourtin et al. [65] for gallium phosphates. The Ga_2O_3 spectrum presents a white line located at 10,372 eV and a second structure at 10,391 eV.

EXAFS spectra of Ga_2O_3 and GM samples showed some similitude. However, the relative intensities of the first two peaks in the *R* space, as well as the second peak located at different *R* positions suggest that although the structures are similar, the gallium phosphate has a distorted structure. This conclusion is also supported by the EXAFS spectra of the two compounds plotted in the *k* space (not shown) that show similar, but still significantly different features.

In the case of GM samples, the first peak centered around 1.75 Å characterizes the tetrahedral environment of the gallium by oxygen (2 Ga–O, 1.81 Å, and 2 Ga–O, 1.82 Å) [65,66]. The second coordination sphere is constituted by four phosphorus atoms characteristic of the Ga–O–P bridges and corresponded to a peak located at 2.82 Å (4 GaP, 3.085 Å) [65,66]. For Ga_2O_3, the first peak is broadened, while the second shell assigned to Ga–O–Ga bridges (3.04–3.45 Å) [65] is evidenced by a higher peak, around 2.88 Å, due to the higher backscattered amplitude of gallium atoms in comparison with the phosphorus one in $GaPO_4$ (Ga–O–P bridges).

In conjunction with the XPS results showing the presence of a P^{5+} peak, these data suggest that the synthesized compounds are gallium phosphates with a distorted Ga_2O_3 crystalline structure.

3.7. TEM

The key point of our work is that using reactive $Ga(OiPr)_3$ and PCl_3 as sources in the synthesis of gallophosphate, small $GaPO_4$ nanoparticles will form at initial synthesis stages that latter will constitute the building block of the structurally robust material. To demonstrate this issue, TEM images at high resolution were obtained. These TEM images are presented in Fig. 8, and they show the presence of well-defined $GaPO_4$ crystallites, hexagonal in shape, with sizes ranging from 8 to 30 nm (Fig. 8a). These pictures are typical for the GM samples. Electron diffraction of these crystallites is shown in Fig. 8b and its corresponding Fourier transformed in Fig. 8c. The last image has allowed measuring the lattice spacing of 3.5 and 6.0 Å along the two directions characteristic for the crystalline structure. This hexagonal structure observed in the Fourier transform of the TEM images of the crystallites is similar to those previously observed for non-conventional Ga_2O_3 samples recently reported by Zhan et al. [67].

The TEM images of some of the GM samples at lower magnification are presented in Fig. 9. The high contrast of the individual gallophosphate crystallites from which the material is constituted can be clearly seen in these figures. The packing of these nanocrystals must lead to a mesoporous texture as indicated by the adsorption data collected in Table 1. These images

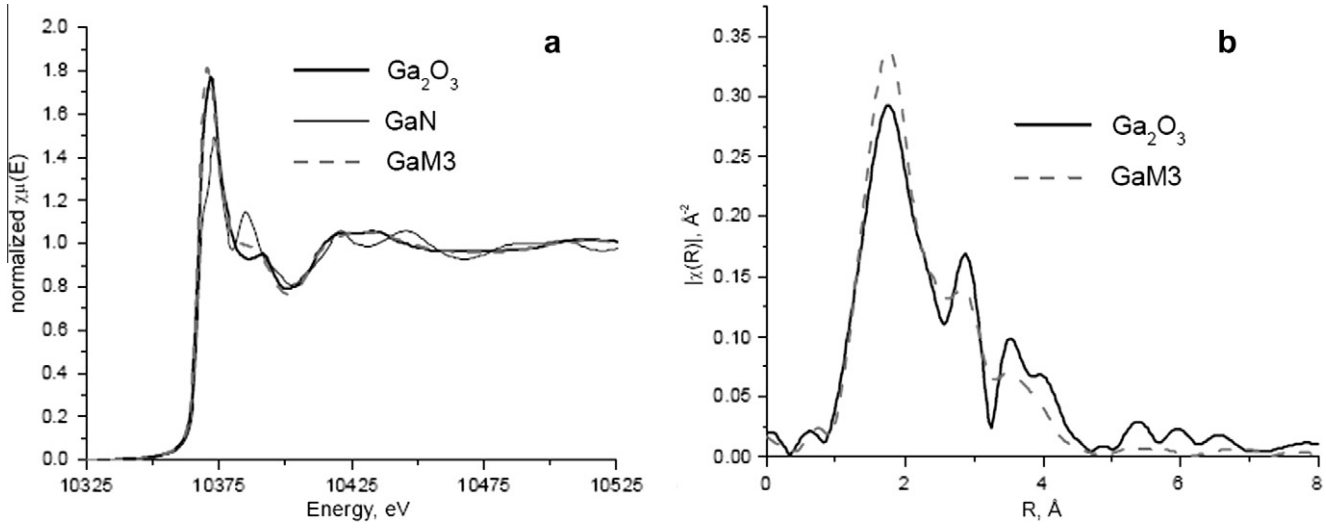

Fig. 7. The EXAFS spectrum of GM3 sample and GaN and Ga_2O_3 reference samples (a), and the EXAFS spectrum in the *R* space of GM3 and Ga_2O_3 samples (b).

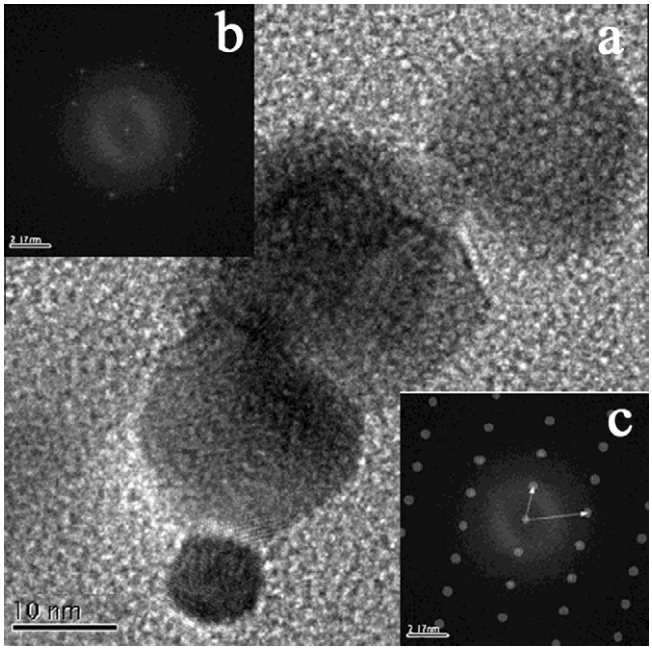

Fig. 8. TEM image showing the morphology of nanometric crystallites (a), the electron diffraction pattern (b) and the corresponding Fourier transform (c) of the GM2 sample.

are consistent with the high surface area of the materials and a compatible with our interpretation of the low degree of periodicity observed in XRD that should correspond to mesoporous samples with wormhole structure.

The use of the different surfactants results in somewhat different packing of these nanocrystals, influencing the porosity and structuring of the building blocks at submicrometric length scale.

3.8. SEM

SEM micrograph of samples GM1–5 is presented in Fig. 10. SEM characterization confirmed the role of the surfactant and synthesis procedure on the structure and morphology. As it can be seen there, GM2 and GM3 show a more homogeneous morphology in which spherical particles predominate. As in other characterization techniques, the morphology of the GM5 and GM6 samples was notably different from that of GM1–4. SEM images are in line with TEM and adsorption–desorption isotherms, indicating that the acid conditions in the synthesis and the use of piperidine and 4-aminopiperidine are not suitable for orienting gallium phosphate crystallites into organized meso-structures (see Fig. 10e).

3.9. XPS

XPS binding energies of Ga3d and P2p levels correspond to Ga^{3+} and P^{5+} in a PO_4 surrounding (Table 4) [68–70]. Generally, XPS binding energies of the Ga3d level in gallium oxide exhibit higher values [71]. Calcination was accompanied in all cases by an increase in P/Ga ratios, which at 550 °C approached the values obtained by chemical analysis of the samples (Table 5). Actually, calcination is the step leading to the stabilization of these mesoporous structures, when the template is released and the external surface probed by XPS corresponds only to gallium phosphate.

Almost no differences were found in this ratio as a function of the directing agent nature or of the preparation route. The Cl/Ga ratios indicated that chlorine was not completely removed by washing or calcination. However, after calcining and washing, it remains only in traces, which is in a perfect concordance with chemical analysis of these samples (Table 5). Nitrogen analysis gave also some insight into the nature of these phosphates. In as-synthesized samples, nitrogen species were found as part of the residual template molecules at ca. 401 eV [72,73] and as nitride at ca. 397 eV [68,74]. After calcination at 550 °C (Table 4), only residual nitride species were present with an intensity slightly reduced compared with that of uncalcined specimen, indicating that part of nitrogen is retained as a constitutive species in the resulting phosphates. However, this nitrogen content in the calcined materials is rather low and consistent with previous reports, indicating that calcination is also leading to the removal of nitrogen (Table 5) [75].

In this regard, the XPS data agree very well with those obtained from the EXAFS and CP-MAS/NMR measurements. EXAFS data provided no arguments in the favor of the formation of gallium nitride or gallium oxide compounds.

3.10. Aerobic oxidation of toluene

As commented earlier, one of possible applications of thermally stable porous gallophosphates will be their use as solid catalyst. We were, therefore, interested in testing the catalytic activity of our GM1–6 samples as heterogeneous catalysts. The reaction selected was the aerobic oxidation of toluene. Benzylic oxidation is in general of wide use that can be effected with stoichiometric oxidants. However, the use of oxygen as oxidizing reagent is of large industrial relevance and would require development of suitable catalysts.

Fig. 11 shows the results in oxidation of toluene on the investigated catalysts. Analysis of the reaction products indicated the formation of only benzyl alcohol and benzaldehyde. Importantly, benzyl ether typically observed as product was not present in the reaction mixture. The conversion of toluene was in the typical

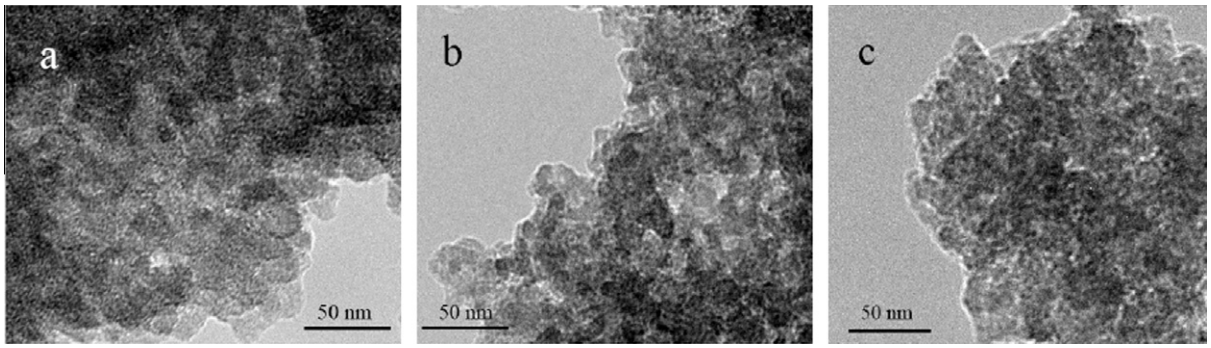

Fig. 9. TEM images of calcined samples GM2 (a), GM3 (b) and GM4 (c) showing the presence of crystallites defining worm-like mesopores.

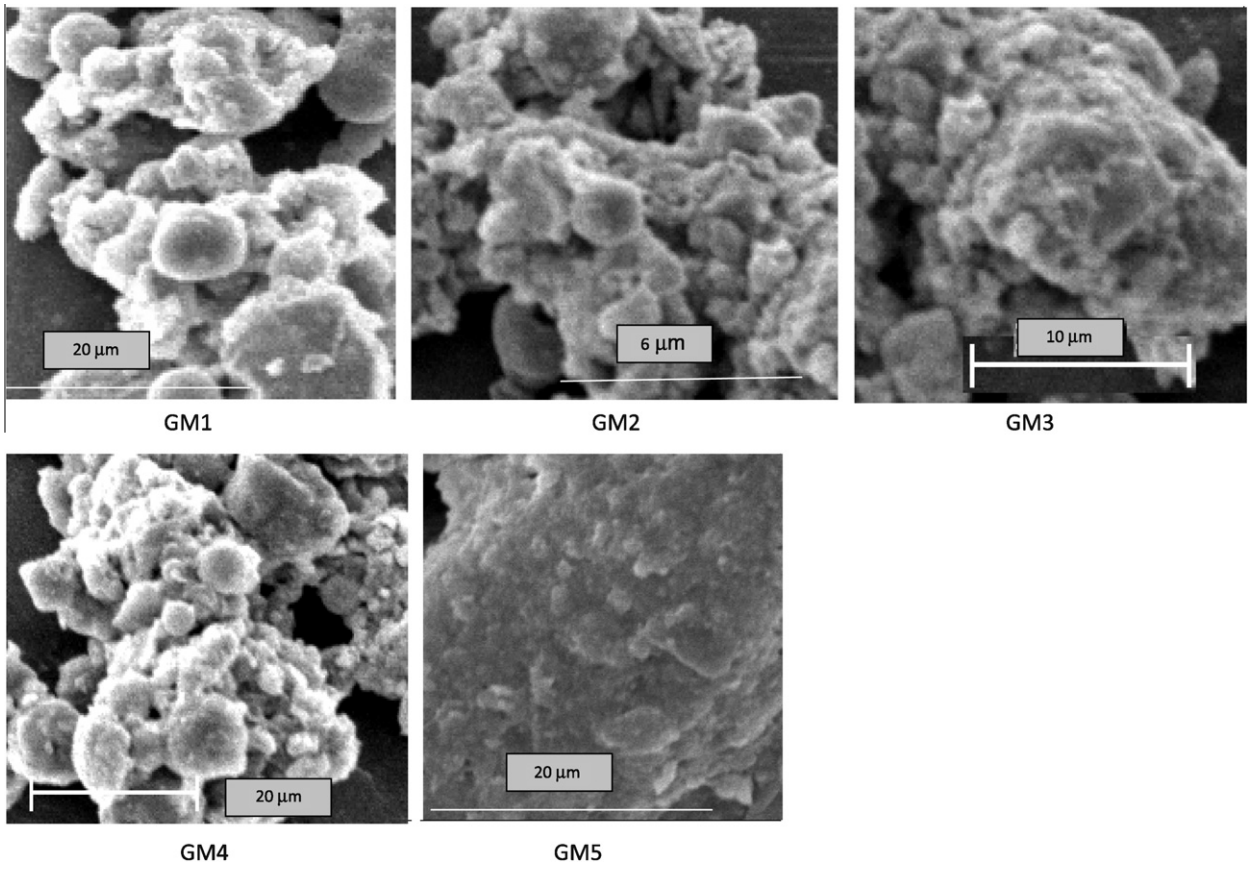

Fig. 10. SEM images of GM samples showing the morphology of the particles constituting the powders. The scale bars of images (a), (d) and (e) is 20 microns, while those of parts (b) and (c) are 6 and 10 microns, respectively.

Table 4
XPS binding energies, and Cl/Ga and P/Ga ratios.

Sample[a]	Binding energy, eV					XPS ratio	
	Ga3d	O1s	N1s	P2p	Cl2p	Cl/Ga	P/Ga
GM1-d	19.6	530.4 531.4	397.2 401.5	133.4	198.9	4.0×10^{-2}	0.13
GM1-c	19.3	530.4 531.4	396.6	133.1	198.7	0.8×10^{-3}	0.80
GM2-d	19.3	530.4 531.4	396.6 401.6	133.1	198.7	5.2×10^{-2}	0.20
GM2-c	19.3	530.4 531.4	396.6	133.1	198.7	0.9×10^{-3}	0.76
GM3-d	19.6	530.4 531.4	397.2 401.5	133.4	198.9	4.0×10^{-2}	0.13
GM3-c	19.3	530.4 531.4	396.6	133.1	198.7	0.8×10^{-3}	0.73
GM4-d	19.3	530.4 531.4	396.6 401.6	133.1	198.7	5.9×10^{-2}	0.20
GM4-c	19.3	530.4 531.4	396.6	133.1	198.7	1.1×10^{-3}	0.76
GM6-d	19.8	530.7	396.8 400.6	133.3	199.0	3.3×10^{-2}	0.21
GM6-c	19.7	530.6	396.8	133.2	198.9	1.2×10^{-3}	0.72

[a] The letter d or c after the sample code corresponds to dried or calcined, respectively.

Table 5
Composition of mesoporous gallium phosphates obtained by chemical analyses.

Sample[a]	Analytic content, %			P/Ga analytic ratio
	Ga	P	N	
GM1-d	13.64	6.20	5.08	1.02
GM1-c	19.03	8.11	0.36	0.95
GM2-d	12.54	5.51	4.46	0.99
GM2-c	18.87	8.16	0.31	0.97
GM3-d	12.71	5.84	4.56	1.03
GM3-c	18.62	8.21	0.33	0.99
GM4-d	12.11	5.37	4.61	0.99
GM4-2c	18.71	8.56	0.35	1.03
GM5-d	11.89	5.32	5.27	1.00
GM5-c	13.09	5.81	0.48	0.99
GM6-d	11.97	5.47	5.66	1.02
GM6-c	13.22	5.83	0.52	0.99

[a] The letter d or c after the sample code corresponds to dried or calcined, respectively.

range of those reported for this reaction for highly active solid catalysts. As it is shown in the figure, the catalytic activity of the GM samples paralleled the surface area of the corresponding GM material. Since all of them are mesoporous, it seems that from the catalytic point of view, all the materials contain the same type of active centers, the difference being mostly on the surface area of the catalyst. This interpretation is in agreement with the NMR and EXAFS characterization that shows identical Ga species. The variations of the preparation procedures modify only the architectures of the spatial ordering constituted in all cases by nanoparticles as primary building blocks.

Fig. 12 shows the product selectivity for each of the six samples. The dominant product was the benzyl alcohol irrespective of the catalyst preparation route. GM2 led to the highest selectivity in benzyl alcohol. The high selectivity to benzyl alcohol is also explained by the fact these materials exhibit almost no acidity that can favor the etherification of the resulted alcohols. The absence

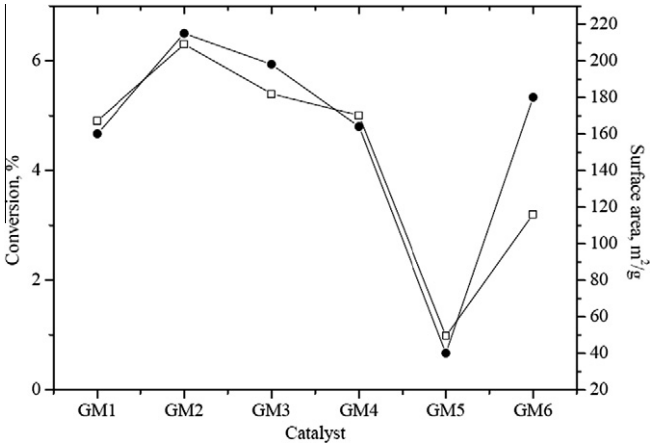

Fig. 11. Variation of the conversion of toluene on the investigated gallium phosphates.

of benzoic acid indicates that the catalysts contain adequate sites to effect the mild oxidation of benzylic sites.

4. Discussion

Several points including our preparation procedure of the GM gallophosphates, their structure, thermal stability and catalytic active deserve especial comments.

4.1. Nature of the precursors and their influence on the synthesis

Most of the gallium phosphate structures that have been synthesized so far have used gallium oxide as precursor. Even in the presence of HF, the disruption of the Ga–O–Ga bonds to the stage of species of single gallium atoms is hard to be achieved under the preparation conditions. The consequence is that not every Ga atom can develop fully the formation of Ga–O–P bonds required in gallophosphates. The use of gallium oxide should favor the presence of Ga–O_x domains in the material.

In the present preparation, the precursors were highly reactive gallium alcoxide and PCl_3. Starting from these compounds, the formation of the Ga–O–P bonds should be easier and dominant minimizing the formation of Ga–O–Ga bridges. PCl_3 reacts rapidly and

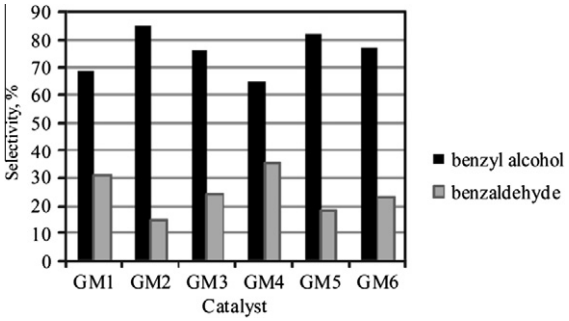

Fig. 12. The variation of the selectivity in the oxidation of toluene.

exothermically in the absence of base with propanol, and products of this substitution reaction are dipropyl phosphonate, propyl chloride and hydrochloric acid:

$$PCl_3 + 3C_3H_7OH \rightarrow (C_3H_7O)_2P(O)H + C_3H_7Cl + 2HCl$$

The obtained HCl catalyses the reaction of $(C_3H_7O)_3P(O)$ with $Ga(OC_3H_7)_3$ and the formation of dipropyl-gallium dipropyl-phosphonate, initiating the condensation. The following equation illustrates a possible primary species having a Ga–O–P bond:

$$(C_3H_7O)_2P(O)H + Ga(OC_3H_7)_3 \rightarrow (C_3H_7O)_2P(O) - Ga(OC_3H_7)_2 + C_3H_7OH$$

Gallium propoxide undergoes in presence of the water traces at the reflux temperature hydrolysis and condensation to dipropyl-gallium dipropyl-phosphonate and other species that subsequently will form the gallophosphate crystallite. This step is promoted by the presence of amines or TMAOH. The following equations illustrate a possible sequence leading to the formation of gallophosphate:

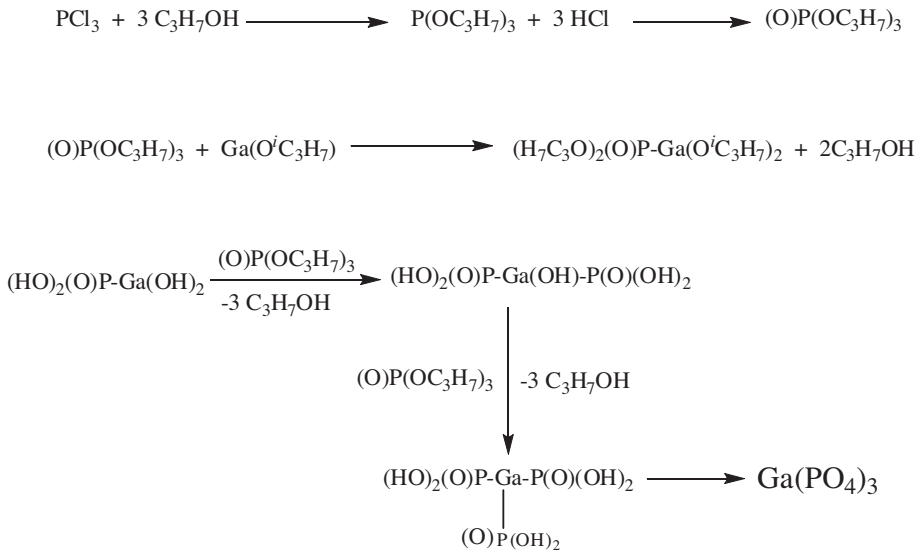

^{31}P and ^{71}Ga MAS NMR spectra and EXAFS brought clear evidences about the formation of Ga–O–P bonds, typical for such mesoporous gallium phosphate structures. Considering the importance of gallium nitrides in electronics, one point of future interest is to determine whether the small residual nitrogen content observed in the samples acts as dopant and introduces electronic states that could be useful for application of the materials in photocatalysis and in electronics. The yellow color of the calcined samples suggests that this possibility is worth of exploration.

4.2. Role of amines and surfactants

In these syntheses, amines exhibit a dual role: initially they participate in the hydrolysis accelerating the formation of gallophosphate crystallites and, subsequently, in a longer time scale producing the spatial organization of the inorganic network of gallium phosphate. When the quaternary salts were used as template, the hydrolysis agent was TMAOH. In all the syntheses, self-assembly of the templates generates micelles in the liquid phase around which the growth of the inorganic network occurs. The final solid particles embed the nanopatches of amines that will imprint the porosity of the material.

Indeed, the combined protocol of hydrolysis of gallium alcoxide in the presence of PCl_3, assisted by surfactants, followed by a microwave treatment resulted in stable porous materials even after calcination at 550 °C that is still unique and opens the way for the use of gallium phosphates as solid catalysts or host matrices. The advantage of using microwave in comparison with the conventional heating is the stabilization of gallium phosphate structures in shorter time. The influence of the heating procedure on the lattice parameter of gallium phosphate has been recently studied [34,35]. Using the microwave, heating is fast and homogenous, this leading to a more adequate growth of nanocrystallites and agglomeration around the template micelles.

To produce stable structures, the role of the template is very important. Kessler's group proposed pyridine as the best surfactant and numerous reports confirmed after that its positive effect. However, in the procedure reported here, it becomes apparent that the template plays a minor role in determining the final structure, this being an additional advantage, since it allows using simple amines. We have been able to generate stable mesoporous structures regardless the nature of the template agent. Typical cationic surfactants such as quaternary salts $C_{16}H_{33}(CH_3)_3NBr$ or N-cetylpyridinium chloride afford gallophosphates with similar wormhole mesopore system as using small amines such as dipropylamine. According to our simple model to rationalize the formation of GM materials, a role of the surfactant is the control of the stacking and aggregation of the nanocrystallites, avoiding the formation of dense, non-porous materials.

This role of the structure-directing agent derives from widely accepted interactions including electrostatic charge matching, hydrogen bonding or dative bond formation between the inorganic precursor and the polar head groups of the structure-directing surfactant micelles [76,77].

As expected, the presence of water favors the formation of the surfactant self-assembly. Thus, the structure of GM4 (the only material in which water was added to the medium) exhibits a higher organization as it was observed by XRD. For GM4, the formation of micropores was also observed (Table 1). Micropores and a smaller surface area have been determined also for dipropylamine (sample GM1) that was indeed not surprising. No micropore formation was determined for the samples GM2 and GM3 synthesized with $C_{16}H_{33}(CH_3)_3NBr$ or $C_{16}PyCl$ solubilized in ethanol.

4.3. Origin of the thermal stability

Based on the images recorded by TEM, we propose that the unique thermal stability of the gallium phosphates synthesized herein derive from the fact that the primary building blocks are crystal nanoparticles and mesoporosity derives from the organization of these robust nanoparticles around the template. There are ample precedents in the literature that have used nanoparticles as primary building blocks to develop mesoporous materials. In this sense, our gallophosphates will be one additional relevant example in which crystalline gallium phosphate nanoparticles are formed in situ during the synthesis.

4.4. Catalytic activity

Preparation of mesoporous gallophosphates has allowed us to test their catalytic activity for a challenging process of large industrial relevance as the aerobic oxidation of alkylaromatics. The results attained are promising and clearly show that the mesoporous gallophosphates offer a large potential in this area. It is worth reminded that toluene is quite inert against oxidation to air, and therefore, only few reports on this subject were published in the literature. For instance, aerobic oxidation of alcohols using gold catalysts can be efficiently promoted in toluene as solvent without noticing the formation of products arising from toluene [78].

For the moment, the oxidation of toluene to benzoic acid uses homogeneous cobalt catalysts in an air pressurized aqueous acetic acid mixture and Mn ions with bromide promoters as catalysts [79]. The use of acetic acid as solvent and promoters led not only to difficulties in the separation of the catalysts and products but also to equipment corrosion. As active catalysts for this reaction were reported metalloporphyrins [80,81], mixed oxides [82], Pt/ZrO_2 [83]. However, these conditions do not allow to stop the oxidation at the stage of benzyl alcohol. In this context, the results presented are remarkable and certainly deserve a separate study to find the scope and limitations of the process.

5. Conclusions

Hydrolysis of gallium alcoxide in the presence of PCl_3 assisted by surfactants, followed by a microwave treatment is leading to the formation of stable mesoporous gallium phosphates constituted by crystalline gallium phosphate nanoparticles. The key step in this process is the prompt formation of Ga–O–P bonds. The formation of Ga–O–P has been demonstrated by ^{31}P and ^{71}Ga MAS NMR and EXAFS experiments. By using this protocol, the formation of the Ga–O–P bonds becomes the dominant progressing spontaneously to the stage of nanoparticles from 5 to 30 nm. These robust primary building blocks undergo stabilization and spatial organization by the template, leading to high surface area and stable materials. This mechanism results in thermal stable porous gallophosphates that so far have been elusive.

We have shown the potential of these novel mesoporous solids by performing the aerobic oxidation of toluene. Even though this aromatic compound is reluctant to undergo benzylic oxidation under mild conditions, our gallophosphates have shown remarkable activity and selectivity. Furthermore, oxidation shows remarkable selectivity toward benzylic alcohol. Thus, it can be anticipated that this report will trigger further research trying to exploit and develop the potential of large-surface area gallophosphates.

Appendix A. Supplementary material

Supplementary data associated with this article can be found, in the online version, at doi:10.1016/j.jcat.2010.11.021.

References

[1] S.T. Wilson, B.M. Lok, C.A. Messina, T.R. Cannan, E.M. Flanigen, J. Am. Chem. Soc. 101 (1982) 1146–1147.
[2] J.B. Parise, Inorg. Chem. 24 (1985) 4312–4316.
[3] J.B. Parise, J. Chem. Soc. Chem. Commun. (1985) 606–607.
[4] J.B. Parise, Acta Crystallogr. C 42 (1986) 144–147.
[5] J.B. Parise, Acta Crystallogr. C 42 (1986) 670–673.
[6] C. Schott-Darie, H. Kessler, M. Soulard, V. Gramlich, E. Benazzi, Stud. Surf. Sci. Catal. 84 (1994) 101–108.
[7] A.K. Cheetham, G. Ferey, T. Loiseau, Angew. Chem. Int. Ed. 38 (1999) 3268–3292.
[8] J.L. Guth, H. Kessler, R. Wey, Stud. Surf. Sci. Catal. 28 (1986) 121–128.

[9] M. Estermann, L.B. McCusker, C. Baerlocher, A. Merrouche, H. Kessler, Nature 352 (1991) 320–323.
[10] S.J. Weigel, R.E. Morris, G.D. Stucky, A.K. Cheetham, J. Mater. Chem. 8 (1998) 1607–1611.
[11] T. Wessels, L.B. McCusker, C. Baerlocher, P. Reinert, J. Patarin, Microporous Mesoporous Mater. 23 (1998) 67–77.
[12] A. Matijasic, J.-L. Paillaud, J. Patarin, J. Mater. Chem. 10 (2000) 1345–1351.
[13] A. Matijasic, B. Marler, J.C. Munoz Acevedo, L. Josien, J. Patarin, J. Chem. Mater. 15 (2003) 2614–2622.
[14] P. Reinert, J. Patarin, B. Marler, Eur. J. Solid State Inorg. Chem. 35 (1998) 389–403.
[15] G. Ferey, C.R. Acad. Sci., Ser. IIc: Chim. 1 (1998) 1–13.
[16] D.S. Wragg, G.B. Hix, R.E. Morris, J. Am. Chem. Soc. 120 (1998) 6822.
[17] J. Patarin, J.-L. Paillaud, H. Kessler, in: F. Schuth, K.S.W. Sing, J. Weitkamp (Eds.), Handbook of Porous Solids, vol. 2, Wiley-VCH Verlag GmbH, Germany, 2002, p. 815.
[18] V.I. Pârvulescu, M. Alifanti, M.H. Zahedi-Niaki, P. Grange, S. Kaliaguine, Stud. Surf. Sci. Catal. 142 (2002) 823–830.
[19] R.I. Walton, T. Loiseau, D. O'Hare, G. Ferey, Chem. Mater. 11 (1999) 3201–3209.
[20] L. Han, Y. Wang, S. Zhang, X. Lu, J. Cryst. Growth 311 (2008) 167–171.
[21] S.-J. Lohmeier, M. Wiebcke, P. Behrens, Z. Anorg. Allg. Chem. 634 (2008) 147–152.
[22] X. Yang, D. Albrecht, J. Caro, Microporous Mesoporous Mater. 112 (2008) 637–640.
[23] A. Merrouche, J. Patarin, M. Soulard, H. Kessler, D. Anglerot, in: M.L. Occelli, H.E. Robson (Eds.), Synthesis of Microporous Materials, Molecular Sieves, vol. 1, Van Nostrand Reinhold, New York, 1992, p. 384.
[24] T. Loiseau, G. Férey, Solid State Sci. 7 (2005) 1556–1560. and references herein.
[25] D.S. Wragg, R.E. Morris, J. Am. Chem. Soc. 122 (2000) 11246–11247.
[26] D. Zhao, J. Sun, Q. Li, G.D. Stucky, Chem. Mater. 12 (2000) 275–279.
[27] S.A. Bagshaw, T.J. Pinnavaia, Angew. Chem. 35 (1996) 1102–1105.
[28] J.N. Cha, G.D. Stucky, D.E. Morse, T.J. Deming, Nature 403 (2000) 289–292.
[29] J. Zhu, B.Y. Tay, J. Ma, Mater. Lett 60 (2006) 1003–1010.
[30] J.K. Shon, S.S. Kong, Y. Kim, J.-H. Lee, W.K. Park, S.C. Park, J.M. Kim, Microporous. Mesoporous. Mater. 120 (2009) 441–446.
[31] Y. Ren, F. Jiao, P.G. Bruce, Microporous Mesoporous Mater. 121 (2009) 90–94.
[32] C.-S. Yang, C.-J. Chen, X.-H. Lin, New J. Chem. 31 (2007) 363–369.
[33] S. Girard, J.D. Gale, C. Mellot-Draznieks, G. Ferey, J. Am. Chem. Soc. 124 (2002) 1040–1051.
[34] P. Armand, M. Beaurain, B. Ruffle, B. Menaert, P. Papet, Inorg. Chem. 48 (2009) 4988–4996.
[35] M. Amri, R.I. Walton, Chem. Mater. 21 (2009) 3380–3390.
[36] J. Lesage, A. Guesdon, B. Raveau, V. Petricek, J. Solid State Chem. 177 (2004) 3581–3589.
[37] F. Bonhomme, S.G. Thoma, T.M. Nenoff, Microporous Mater. 53 (2002) 87–96.
[38] D.W. Breck, Zeolite Molecular Sieves: Structure, Chemistry and Use, John Wiley and Sons, New York, 1974.
[39] H. van Bekkum, E.M. Flanigen, J.C. Jansen (Eds.), Introduction to Zeolite Science and Practice, Elsevier, Amsterdam, 1991.
[40] A. Corma, H. Garcia, Eur. J. Inorg. Chem. 6 (2004) 1143–1164.
[41] P. Atienzar, S. Valencia, A. Corma, H. Garcia, ChemPhysChem 7 (2007) 1115–1119.
[42] P. Atienzar, M. Navarro, A. Corma, H. Garcia, ChemPhysChem 10 (2009) 252–256.
[43] M. Alvaro, J.F. Cabeza, A. Corma, H. Garcia, E. Peris, J. Am. Chem. Soc. 129 (2007) 8074–8075.
[44] M. Alvaro, J.F. Cabeza, D. Fabuel, A. Corma, H. Garcia, Chem. Eur. J. 13 (2007) 3733–3738.
[45] H. Du, J. Chen, W. Pang, Stud. Surf. Sci. Catal. 105 (1997) 397–404.
[46] M. Elanany, A.V. Larin, B.-L. Su, D.P. Vercauteren, Stud. Surf. Sci. Catal. 162 (2006) 339–346.
[47] Y. Chen, D. Ciuparu, S. Lim, Y. Yang, G. Haller, L. Pfefferle, J. Catal. 225 (2004) 453–465.
[48] E.A. Stern, M. Newville, B. Ravel, Y. Yacoby, D. Haskel, Physica B 209 (1995) 117–120.
[49] K.S.W. Sing, D.H. Everett, R.A. Haul, L. Moscou, R.A. Pierotti, J. Rouquerol, T. Siemieniewska, Pure Appl. Chem. 57 (1985) 603–619.
[50] W.C. Conner, S. Christensen, H. Topsoe, M. Ferrero, A. Pullen, in: J. Rouquerol, F. Rodriguez-Reinoso, K.S.W. Sing, K.K. Unger (Eds.), Characterization of Porous Solids III, Elsevier, Amsterdam, 1994, p. 151.
[51] F. Rouquerol, J. Rouquerol, K.S.W. Sing, Adsorption by Powders and Porous Solids, Academic Press, London, 1999. p. 204.
[52] S.-I. Hirano, P.-C. Kim, J. Mat. Sci. 25 (1990) 4772–4775.
[53] M. Haouas, F. Taulelle, N. Prudhomme, O. Cambon, J. Cryst. Growth 296 (2006) 197–206.
[54] S. Delsarte, P. Grange, T.C.P. Grobet, P. Jacobs, J. Phys. Chem. B 107 (2003) 6504–6510.
[55] S. Delsarte, V. Serin, A.M. Flank, F. Villain, P. Grange, J. Solid State Chem. 163 (2002) 163–177.
[56] A. Marquez, J. Fernandez Sanz, J.A. Odriozola, J. Non-Cryst. Solids 263 (2000) 189–194.
[57] V. Montouillout, C.M. Morais, A. Douy, F. Fayon, D. Massiot, Magn. Reson. Chem. 44 (2006) 770–775.
[58] D. Massiot, T. Vosegaard, N. Magneron, D. Trumeau, V. Montouillout, P. Berthet, T. Loiseau, B. Bujoli, Solid State NMR 15 (1999) 159–169.
[59] F. Taulelle, A. Samoson, T. Loiseau, G. Ferey, J. Phys. Chem. B 102 (1998) 8588–8598.
[60] V.A. Nikanorov, A.D. Rogachev, M.V. Galakhov, T.M. Shcherbina, D.V. Zagorevskii, V.I. Rozenberg, O.A. Reutov, V.V. Kaverin, V.P. Yurev, Russ. Chem. Bull. 45 (1996) 424–429.
[61] S.K. Kulshreshtha, O.D. Jayakumar, V. Sudarsan, J. Phys. Chem. Solids 65 (2004) 1141–1146.
[62] S.R. Zhai, W. Wei, D. Wu, Y.-H. Sun, Catal. Lett. 89 (2003) 261–267.
[63] C. Aprile, L. Teruel, M. Alvaro, H. Garcia, J. Am. Chem. Soc. 131 (2009) 1342–1344.
[64] Y. Zhang, J. Yuan, J. Le, L. Song, X. Hu, Solar Energy Mater. Solar Cells 93 (2009) 1338–1344.
[65] F. Tourtin, A. Ibanez, A. Haidoux, E. Philippot, Thin Solid Films 279 (1996) 59–65.
[66] A. Goiffon, J.C. Jumas, M. Maurin, E. Philippot, J. Solid State Chem. 61 (1986) 369–384.
[67] J. Zhan, J. Hu, F. Xu, D. Golberg, Small 1 (2005) 883–888.
[68] J. Hedman, N. Martensson, Phys. Scripta 22 (1980) 176–178.
[69] F.J. Grunthaner, P.J. Grunthaner, R.P. Vasquez, B.F. Lewis, J. Maserjian, A. Madhukar, J. Vac. Sci. Technol. 16 (1979) 1443–1453.
[70] R. Franke, Th. Chasse, P. Streubel, A. Meisel, J. Electron Spectrosc. Relat. Phemon. 56 (1991) 381–388.
[71] M. Nieminen, L. Niinisto, E. Rauhala, J. Mater. Chem. 6 (1996) 27–31.
[72] W.E. Swartz, R.C. Gray, J.C. Carver, R.C. Taylor, D.M. Hercules, Spectrochim Acta A30 (1974) 1561–1572.
[73] B.J. Lindberg, J. Hedman, Chem. Scripta 7 (1975) 155–166.
[74] R. Carin, J.P. Deville, J. Werckmann, Surf. Interface Anal. 16 (1990) 65–69.
[75] F. Bonhomme, S.G. Thoma, T.M. Nenoff, Microporous Mesoporous Mater. 53 (2002) 87–96.
[76] S.-S. Kim, Y. Liu, T.J. Pinavaia, Microporous Mesoporous Mater. 44–45 (2001) 489–498.
[77] H. Li, Q. Zhao, Y. Wan, W. Dai, M. Qiao, J. Catal. 244 (2006) 251–256.
[78] A. Abad, A. Corma, H. Garcia, Chem. Eur. J. 14 (2008) 212–222.
[79] H. Holtz, L. Gardner, Phillips Petroleum Co., US Pat. 4088823, 1978.
[80] C.-C. Guo, Q. Liu, X.-T. Wang, H.-Y. Hu, Appl. Catal. A: Gen. 282 (2005) 55–59.
[81] G. Huang, J. Luo, C.C. Deng, Y.A. Guo, S.K. Zhao, H. Zhou, S. Wei, Appl. Catal. A: Gen. 338 (2008) 83–86.
[82] X. Li, J. Xu, L. Zhou, F. Wang, J. Gao, C. Chen, J. Ning, H. Ma, Catal. Lett. 110 (2006) 255–260.
[83] M. Ilyas, M. Sadiq, Catal. Lett. 128 (2009) 337–342.
[84] P. Labéguerie, M. Harb, I. Baraille, M. Rérat, Phys. Rev. B 81 (2010) 045107.